

www.acsanm.org Article

# Laser-Induced Graphene-Based Smart Textiles for Wireless Cross-Body Metrics

Huiting Qin, Amirhossein Hajiaghajani, Alberto Ranier Escobar, Amir Hosein Afandizadeh Zargari, Abel Jimenez, Fadi Kurdahi, and Peter Tseng\*



Cite This: ACS Appl. Nano Mater. 2023, 6, 19158-19167



**ACCESS** I

III Metrics & More

Article Recommendations

SI Supporting Information

ABSTRACT: Textile-based sensors have emerged as a promising technology for enabling low-burden, personalized, and on-body biometrics. However, current textile sensors often lack multimodal or multipositional sensing capabilities, are challenging to fabricate at scale, and are not seamlessly integrated into textile-borne readout systems. We report textile-integrated, laser-induced graphene (LIG) sensors for multiparametric biometrics monitoring. The LIG sensors are designed with custom patterns specific to different stimuli—strain, humidity, and temperature demonstrated herein—and exhibit tunable sensitivity through control of the pattern geometry and the laser power used during LIG conversion. These sensors are highly sensitive to changes in resistance, rapidly respond to stimuli (<5 s), and exhibit remarkable stability for at least 1000 cycles. Lastly, such sensors are synthesized



alongside magnetic metamaterials and are seamlessly coupled with flexible near-field communication systems directly on textile. This enables fully integrated "smart" clothing capable of battery-free, wireless monitoring of cross-body metrics. Such protocols represent a straightforward, accessible strategy for directly incorporating multiple sensor and network elements into on-demand textiles for advanced human body measurements.

KEYWORDS: smart textile, laser-induced graphene, metamaterial, battery-free near-field communication, multiparameter

## INTRODUCTION

Point-of-care, wearable/implantable devices are an essential technology class within precision health. Device-enabled, realtime biometrics monitoring provides valuable feedback on personal health and early warnings of poor body function. Significant research effort has been placed on sensing technologies and body-interfacing systems 2-7 that potentially distribute around (and within) the body while collecting local biomechanical/chemical information. Within wearable devices, textile-based sensors<sup>8-17</sup> have emerged as a promising technology for sensing and transducing in various research fields (mechanical sensing and translating machine interactions).<sup>20</sup> Compared to traditional wearable sensors, textile-borne sensors possess several advantages in terms of user comfort, wearability, and long-term monitoring capabilities. Textile sensing elements are often characterized by their flexibility, lightweight nature, and integrability into everyday clothing.<sup>21</sup> The integration of such sensors not only enhances user comfort but can also reduce user burden and improve compliance with real-time wearable monitors.<sup>22</sup> Additionally, advances in textile sensors include improved durability, washability, and resistance to environmental factors, which may further facilitate their widespread adoption in health monitoring applications.<sup>23</sup>

Despite the numerous advantages of textile-borne sensors, certain challenges and limitations hinder their widespread adoption in health monitoring applications. One concern is the variability in signal quality and sensitivity, which may arise from factors such as textile stretching, bending, and pressure during regular use.<sup>24</sup> Such variability can result in inconsistent and unreliable data collection. 25 Furthermore, textile sensor readout presents significant challenges, as sensors often require monitoring by battery-powered microsystems that do not integrate well into clothing with existing protocols—this is still an ongoing area of research.<sup>26</sup> The lack of standardized manufacturing has also proven to be an impediment. For example, the current development of textile sensors often requires the integration of high-quality conductive materials (conductive and flexible fibers or yarns) into the fabric structure using techniques such as weaving, knitting, or embroidering. These processes can be intricate and time-

Received: August 4, 2023 Accepted: September 27, 2023 Published: October 6, 2023





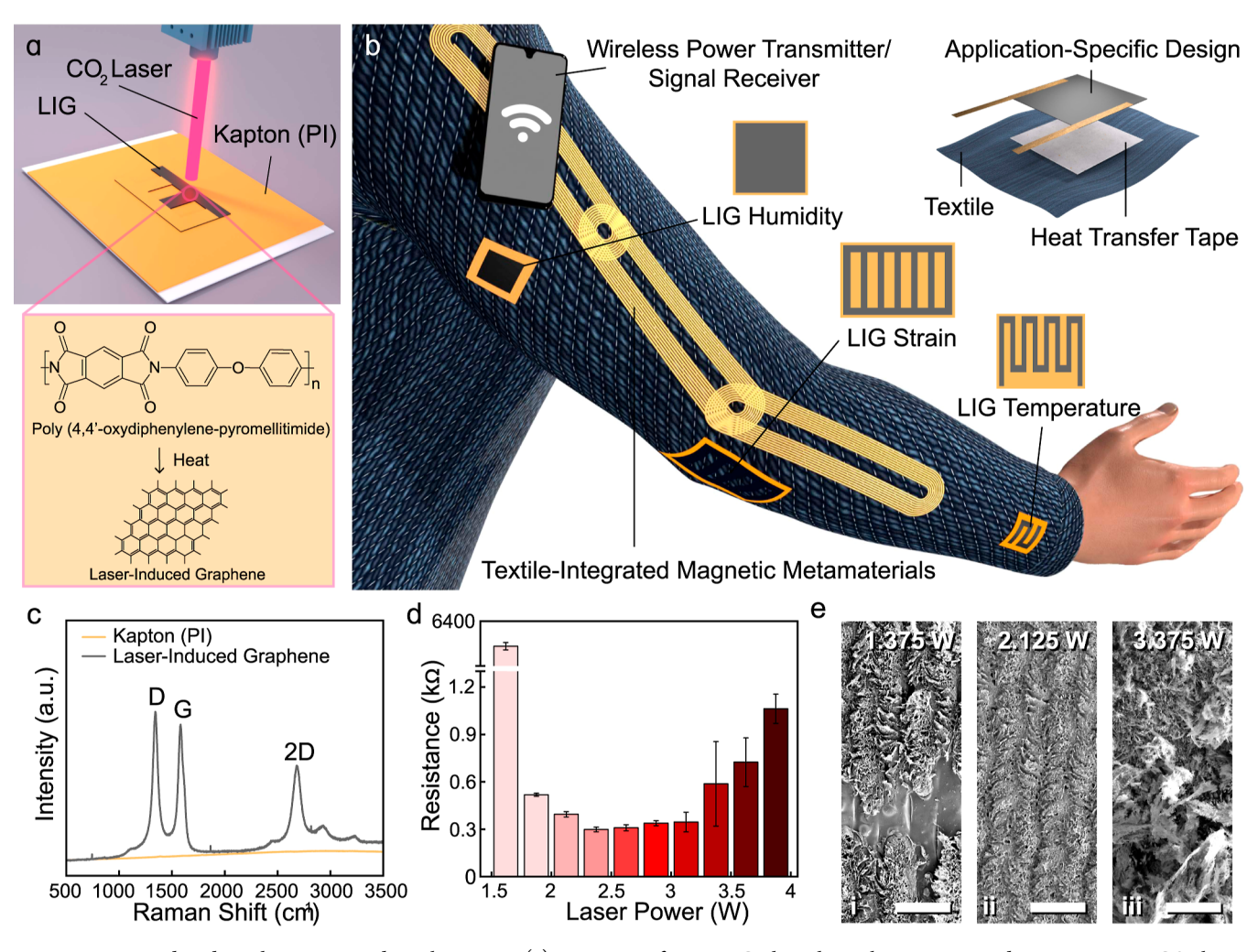


**Figure 1.** Laser-induced graphene-patterned textile sensors. (a) Depiction of PI-to-LIG photothermal conversion under exposure to a  $CO_2$  laser. (b) Schematic of patterned LIG-based, multifunctional textile sensors cointegrated with textile-integrated metamaterials for cross-body networking. (c) Raman spectra of PI film before laser exposure and LIG after successful PI conversion. (d) Resistance of LIG samples converted from PI film at varying laser powers. (e) Surface morphology of LIG samples at three distinct laser power values (scale bar = 100  $\mu$ m).

consuming, often requiring specialized equipment and skilled labor. Scaling up the production of textile sensors can also be an issue, as many manufacturing techniques can be laborintensive. Additionally, the need for customizability to meet specific person-to-person application requirements further complicates these sensors. Lastly, the manufacturing processes of textile sensors may involve the use/deposition of chemicals and nanomaterials or generate waste materials that pose environmental risks.

Here, we propose a facile strategy fusing multiple sensor, network, and readout technologies into "smart" textiles capable of wireless, battery-free readout of cross-body metrics. At the core of our approach are laser-induced graphene (LIG)-based textile sensors. Since its initial discovery, LIG has garnered significant interest owing to its facile synthesis, scalability, and multipurpose applications (including supercapacitors, <sup>30,31</sup> electrocatalysis, <sup>32,33</sup> wearable strain sensors, <sup>34–36</sup> air filters, <sup>37</sup> and other fields). Here, we extend on recent developments in textile-borne LIG sensors <sup>11,44–47</sup> to study how such sensors can be synthesized, designed, integrated within multilayers (imparting protection, rigidity, and improved selectivity) on clothing, and wirelessly interrogated. In combination, such strategies enable selective, battery-free monitoring of various parameters during motion; those

demonstrated here include humidity, temperature, pulse, and strain.

Finally, these on-demand sensors are synthesized alongside magnetic metamaterial network elements we recently developed.<sup>48</sup> Such networks support intermediate-range, magnetoinductive waves that passively direct wireless power and information across the body. These networks exhibit characteristics similar to those of the LIG sensors as they are composed of discrete, customizable elements that can be built on-demand to fit user needs in sensing or shape. We demonstrate facile protocols by which multiple sensors, networks, and interrogating systems can be cointegrated on textiles in a single heat press step. Sensor systems distributed at various positions across the body are networked by a metamaterial network and can be used for local measurements. The resulting integrated "smart" clothing exhibits battery-free, wireless comonitoring of cross-body metrics that can be built on-demand and adapted to individual requirements. Overall, this approach represents a straightforward, accessible strategy for leveraging the flexibility of LIG for advanced human body measurement.

LIG Characterization and Textile Sensor Fabrication. The process of converting a polyimide (PI) film into an LIG is initiated by irradiating the film with a commercial laser cutter (Figure 1a). Laser irradiation, achieved via laser scribing,

beneficial for its simplicity and cost-effectiveness, can be conducted under ambient conditions. Upon exposure to the laser, the PI film undergoes rapid localized heating, which breaks imide rings and produces volatile gaseous products, such as carbon dioxide ( $\rm CO_2$ ) and water vapor ( $\rm H_2O$ ). Concurrently, the aromatic and conjugated structures in PI are transformed into an sp²-hybridized carbon network, which constitutes the graphene lattice.

The laser irradiation process allows for the rapid generation of custom designs that can be optimized to augment the performance of sensors when measuring different environmental conditions. Here, we focus on optimizing textile-LIG for three key local body measurements of strain, temperature, and humidity/moisture (Figure 1b). For strain-sensing, a shutter pattern can improve sensitivity as it incorporates multiple resistors in parallel that retain functionality even if damaged and maximizes gauge factor (GF).<sup>50</sup> For temperature sensing, a serpentine pattern exhibits high sensitivity while minimizing the total sensor length and maximizing the local heat transfer. Additionally, this allows for better strain accommodation during thermal expansion and contraction.<sup>51</sup> For humidity sensing, a simple square-shaped sensor can maximize the area-to-perimeter ratio, enabling more water absorption while being simple to scale for increasing sensitivity.

To integrate LIG patterns onto the textile, we used a heat press treatment with heat transfer tape as an intermediary to create a seamless connection between the LIG patterns and the textile (Figure S1a). Application-specific layering and design strategies can be employed to further improve the adaptability and utility of textile sensors. Silicone is employed as an encapsulation layer for the temperature and strain sensors, shielding them from the environment. For temperature and humidity sensors, an optional thin 3D-printed support can further enhance stability by mitigating strain variations. Lastly, for humidity sensors, a small portion of liquid tape protects connectors from the detrimental effects of moisture (Figure S1b-d).

Graphene formation was validated using Raman spectroscopy on PI before and after processing (Figure 1c). The Raman spectrum of LIG reveals three peaks: the D peak (1350 cm<sup>-1</sup>), indicating intervalley phonon and defect scattering; the G peak (1580 cm<sup>-1</sup>), a primary in-plane vibrational mode; and the 2D peak (2690 cm<sup>-1</sup>), indicating the second-order overtone of an in-plane vibration. These are consistent with published graphene Raman spectra and confirm conversion into graphene during our laser scribing process.<sup>45</sup>

PI undergoes distinct electrical transformations as the incident laser power is modulated (Figure 1d). If the laser power is less than 1.875 W, PI fails to convert into LIG and maintains high resistance (Figure S2a). Just above 1.875 W, there is a significant decrease in the film resistance accompanying a black coloration (Figure S2b,c). The surface morphology exhibits a convoluted reticular porosity indicative of successful PI-to-LIG conversion (Figure 1e(i,ii) and S3a-c). This decrease in the resistance is maintained until the power reaches 3.125 W, at which point the resistance begins to increase. We attribute this increase in resistance to the introduction of small cracks resulting from elevated local temperatures that weaken and break C-O, C=O, and C=N bonds in the PI film (Figure 1e(iii)). When the power exceeds 3.875 W, LIG is reduced to ash (Figure S2d).

Characterization of the LIG Strain Sensors. We first validated our synthesized LIG as a strain sensor. The dynamic

responses of the LIG textile to repeated stretch/release cycles with the different applied strains were tested (Figure 2a). The

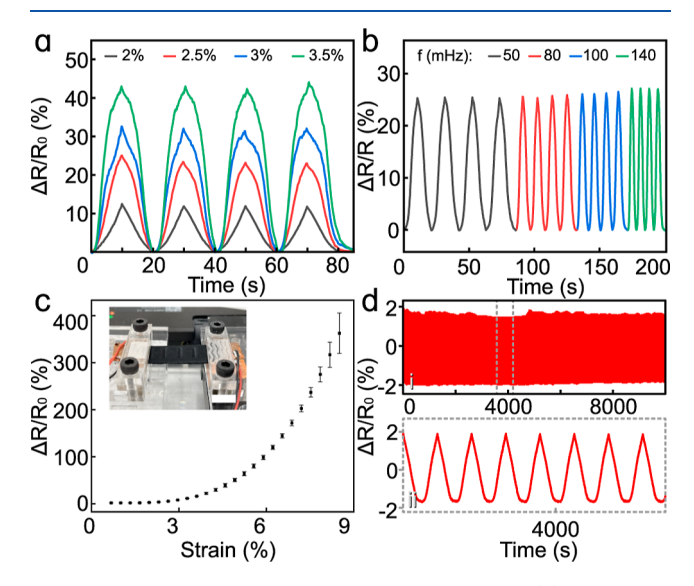


**Figure 2.** Characteristics of the LIG strain sensors. (a) Change in resistance versus time, showcasing stability and sensitivity. (b) Change in resistance versus time, depicting the frequency sensitivity. (c) Change in resistance versus strain graph, depicting sensor sensitivity (scale bar = 1 cm). (d) Repeatability measurements of the LIG strain sensors over 1000 cycles.

sensor response to stimuli at various frequencies of 50, 80, 100, and 140 mHz exhibited minimal resistance fluctuation (Figure 2b). Such resilience is essential for body monitoring. Figure 2c illustrates the sensitivity of the strain sensor and, notably, its increasing sensitivity as the sensor is further strained. This increasing sensitivity is made clear when analyzing three linear regions in the graph, 0–2, 2–4.5, and 4.5–8%, with extracted gauge factor (GF) values of 3.5, 20.19, and 114, respectively. By altering the LIG pattern geometry, the sensor GF yields tunable changes in sensitivity and stretchability (Figure S4a). These parameters can be further tuned by careful selection of the PI-to-LIG laser power, highlighting precise control over the performance of LIG textile sensors (Figure S4b).

We further validated the mechanical stability under a cyclic strain of 2.5% to confirm sensor durability (Figure 2d). To demonstrate the potential of LIG-based, wearable textile sensors in on-body applications, we conducted experiments to evaluate the sensor's ability to distinguish between diverse motions (Figure 3). Sensors were integrated into clothing above three distinct areas of the arm-wrist, inner elbow, and outer elbow-and the user was instructed to perform various movements. Figure 3a-c showcases wrist motions (flexion, extension, and ulnar deviation) specifically chosen to assess sensor reliability, efficacy (as defined by their ability to differentiate motions), and sensitivity. During wrist extension, the LIG strain sensor displayed opposing sensing behavior (decreased relative resistance in response to sensor deformation) and a significant change in relative resistance (26%) when compared to wrist flexion (20%) due to the more significant sensor deformation caused by the larger bending angle. As expected, ulnar deviation resulted in a reduced signal due to the lower strain induced by the out-of-plane motion, yet the sensor remained capable of discerning this signal nonetheless. This sensitivity is further supported by the

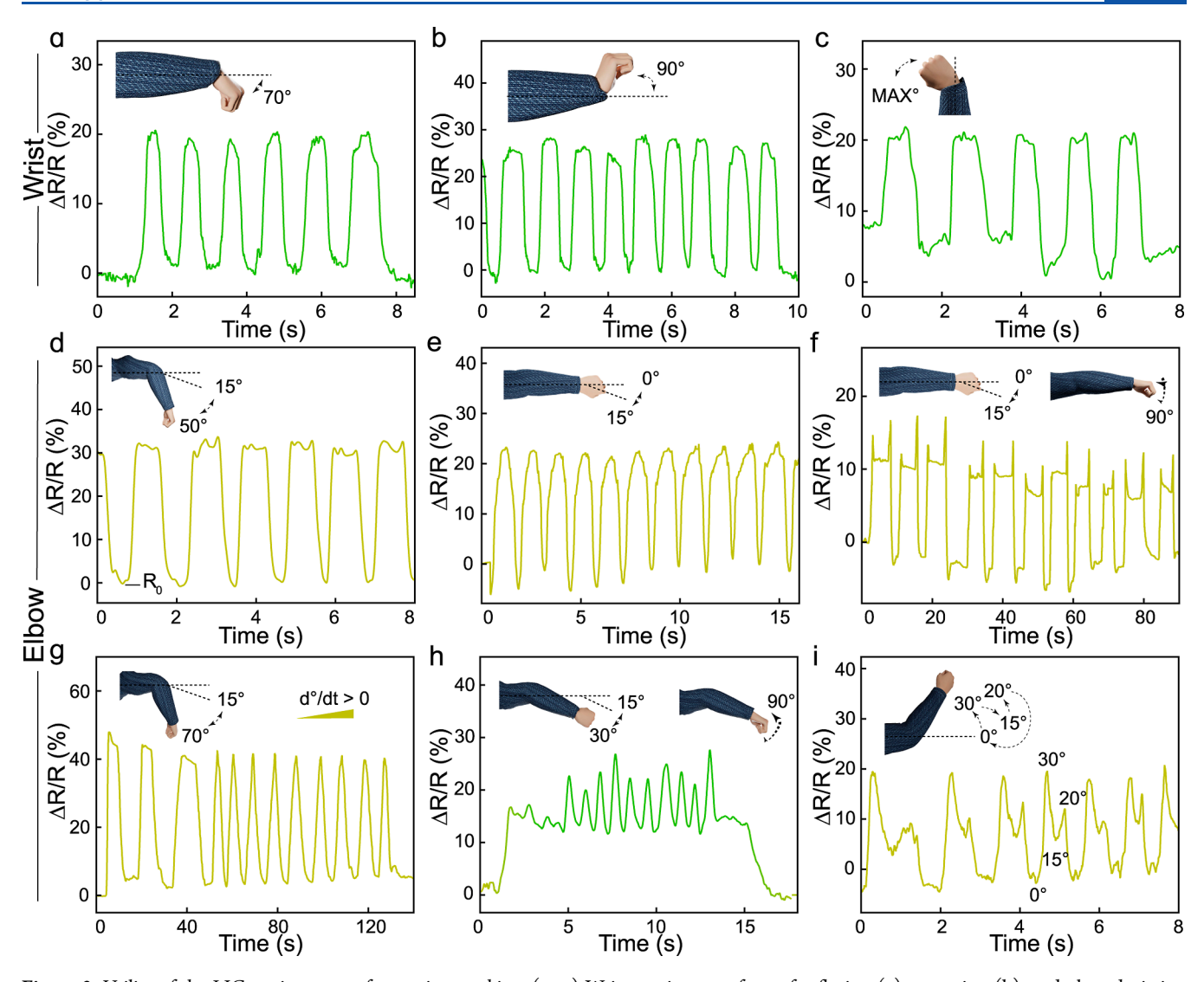


Figure 3. Utility of the LIG strain sensors for motion tracking. (a-c) Wrist motion waveforms for flexion (a), extension (b), and ulnar deviation (c). (d-i) Elbow motion waveforms for flexion (d), extension (e), extension and supination (f), flexion with increasing flexion rate (g), extension and wrist supination (h), and a bicep curl analogue with an incorporated partial repetition (i).

sensor's ability to detect subtle stain variations induced by a subject's pulse (Figure S5).

We further tested the strain sensor response to flexion, extension, and supination motions with a strain sensor inside or outside the joint. Sensor response remained stable across basic motions and could detect elbow supination with the sensor located inside the joint (Figure 3d-f), a motion with lower sensor deformation compared to ulnar deviation. Additionally, we assessed the sensor's response rate to increasing flex rate and found that these sensors can readily discern complex motions (Figure 3g, sensor outside the joint). In Figure 3h, the subject, equipped with a strain sensor on the outside of the elbow joint, was instructed to flex their elbow, followed by a repetitive wrist supination before returning to the initial position. Wrist supination could be captured by the elbow sensor via forearm motions, illustrating the sensor's ability to detect multijoint movements with ease. Figure 3i illustrates repeated signals obtained from a sequence of movements intended to mimic a bicep curl with an incorporated pause. Beginning from a fully extended position, the subject was instructed to flex their elbow to 30°, extend to 15°, and flex to 20° before returning to their initial position.

The sensor could detect minute differences between the various flex states. These results highlight the effectiveness and versatility of LIG-based textile sensors in monitoring human motion across a range of potential applications.

Based on these findings, we further explored the strain sensor's continuous service capability. This was achieved by conducting routine tests once per day using the same sensor, which was then stored under ambient conditions until the next recording (Figure S6a,b). The LIG strain sensor demonstrated exceptional stability, maintaining effective operation for at least 40 days with minimal resistance fluctuations below 0.1%. Furthermore, the sensor's outstanding reproducibility attests to the efficacy of our design strategy (Figure S7). These findings indicate that the LIG sensor can sustain consistent performance, long-term mechanical stability, and high accuracy over prolonged periods of use.

Characterization of the LIG Ambient Sensors. Laser-induced graphene possesses an intricate, interconnected porous network that contributes to LIG's remarkable material properties, including its ability to respond to humidity and temperature variations. Capitalizing on these attributes, we explored the potential of LIG for humidity and temperature-

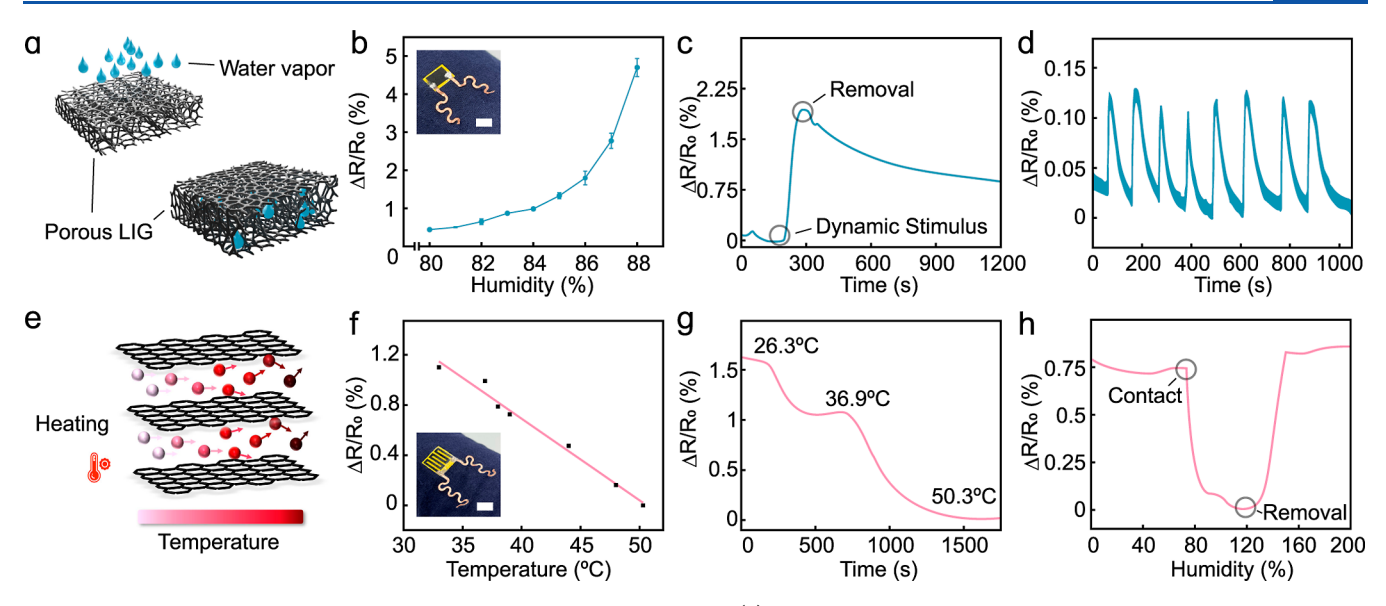


Figure 4. Characterization of the LIG humidity and temperature sensors. (a) Infiltration of water vapor into porous LIG induces resistance changes. (b) Change in resistance versus relative humidity. (c) Dynamic response of the LIG humidity sensor when exposed to large and (d) small stimuli. (e) Motility of atoms within the LIG structure resulting from temperature changes. (f) Calibration plot and (g) dynamic response of the LIG-based temperature sensor in the physiological temperature range. (h) Dynamic response of an LIG temperature sensor upon contact with and removal from the human body. (All scale bars = 5 mm).

sensing applications by optimizing sensor-on-textile performance through engineered multilayers.

The porous nature of LIG allows for efficient adsorption and desorption of water molecules, which enables the material to respond to changes in ambient humidity. Adsorption causes an increase in the overall mass of LIG, leading to a measurable change in its electrical resistance via swelling of the laserinduced graphene (Figure 4a). To evaluate the performance of the LIG humidity sensor, the sensor was placed in a humiditycontrolled environment, where the humidity varied. The humidity sensor demonstrated a rapid and stable response to humidity variations, with a sensitivity of 0.525% relative humidity (RH) (Figure 4b). The sensitivity of the LIG-based humidity sensor increases rapidly at high humidity levels because the swelling process becomes more pronounced. We investigated the dynamic response of the LIG textile to humidity while worn by human subjects. When applying a swift, high humidity from the surroundings ( $\sim$ 90%), the sensor shifted rapidly and slowly returned to its initial state upon removal of the stimulus (Figures 4c and S8a,b). We also observed the sensor's fast response to fluctuations in humidity when subjected to a pulse stimulus (Figure 4d).

LIG's porous structure also contributes to efficient thermal conductivity, allowing it to respond effectively to temperature changes. As the temperature increases, conductivity improves due to heightened electron-phonon scattering and the accelerated thermal velocity of electrons in sandwiched layers. To evaluate the temperature sensor performance, we positioned the LIG sensor on a hot plate with an silicone stage for stabilization and calibration. The temperature sensors display a distinct, rapid, and stable response to temperature fluctuations, with a sensitivity of -0.06% °C<sup>-1</sup>, indicative of LIG's negative temperature coefficient behavior (Figure 4f). We further investigated the dynamic temperature response of the LIG temperature sensor while worn by a subject. A preheated silicone pad was used as a heat stimulus and applied to the subject's arm, where the LIG temperature sensor was placed. The resistance of LIG decreased significantly upon

contact with the heat stimulus and returned to its initial status once the stimulus was removed (Figure 4h). To evaluate the stability of the temperature sensor during human motion, the multilayer sensor signal was recorded under dynamic temperature stimulus conditions while the subject moved their arms (Figure S8c). The LIG temperature sensor maintains accurate and consistent readings even during dynamic activities, thus highlighting its potential for reliable temperature monitoring in wearable applications.

LIG-Based, Integrated "Smart" Clothing for Cross-**Body Metrics.** One current key limitation of textile sensors is the need for readout systems. Sensors at different nodes are typically wired to microelectronic systems that require printed circuit boards and rigid batteries which rarely appear in published images and are not integrated into clothing. To address this limitation, we first designed ultralightweight, flexible near-field communication (NFC) boards to interface with each sensing node directly. NFC readout facilitates wireless and seamless high-data-rate powering and monitoring of sensors that are outside the capabilities of traditional bluetooth and allows sensors to be monitored without rigid batteries. We employ a facile approach to wirelessly power and network multipositional LIG sensors, ultimately enabling battery-free, cross-body metrics. LIG sensors are cointegrated on textiles with magneto-inductive metamaterials that are flexible, robust (minimal interconnects and no long-range wiring), and easy to extend.<sup>48</sup> This consists of arrays of thinfilm resonators tuned to transmit in the NFC band. These metamaterials exhibit synergistic qualities with LIG sensors, as they can be similarly designed on-demand, placed as needed to meet various applications, and built into textiles using simple heat-press processes. A simple NFC-enabled smartphone or dedicated NFC reader can be placed anywhere near the metamaterial for network measurement.

The body area network (BAN) and LIG sensors are cointegrated into clothing in a single step (Figure 5a) with sensors custom-designed to locally interface with the replaceable, flexible NFC board (Figure 5b). The sensor

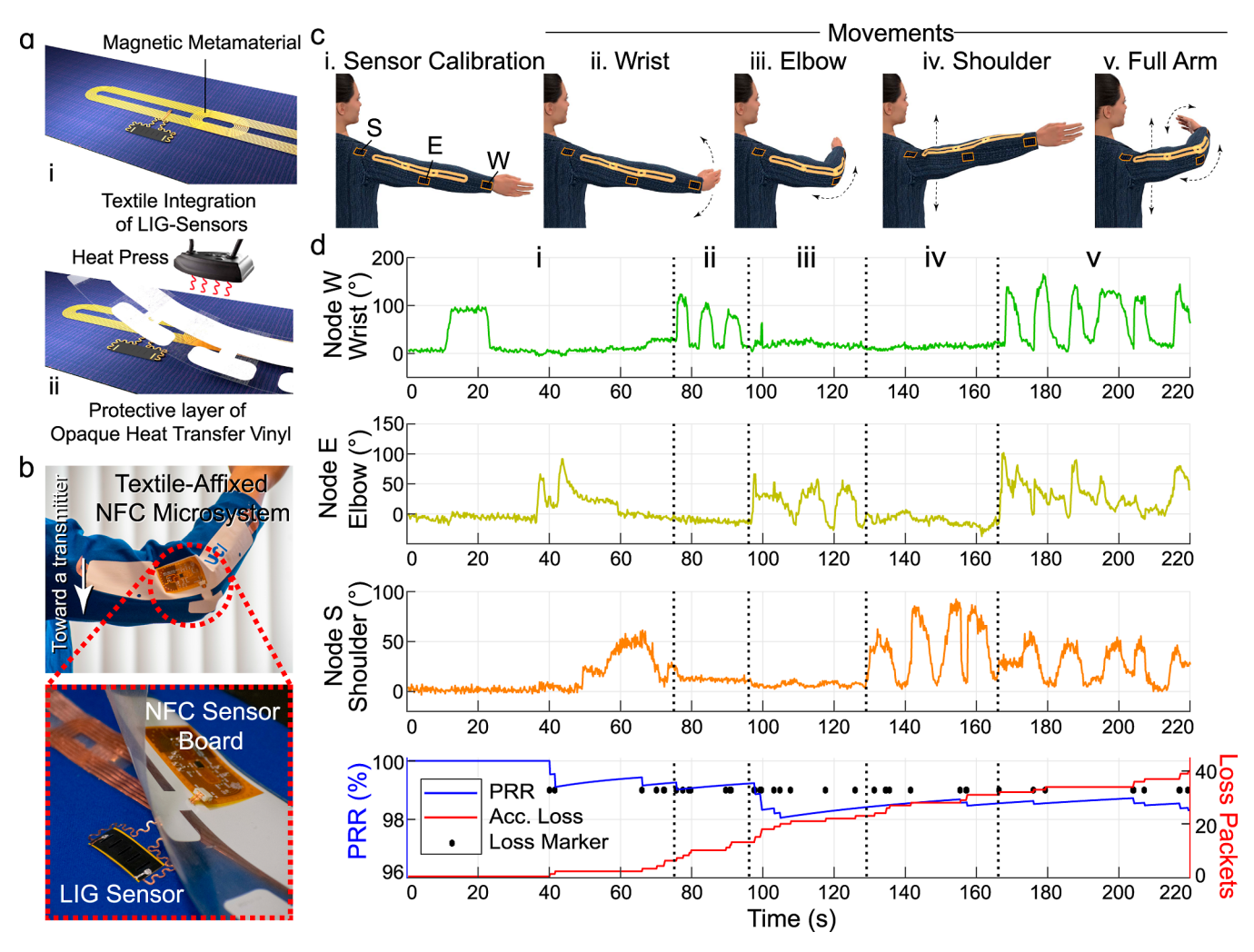


Figure 5. Multinode posture monitoring via LIG-based, "smart" battery-free clothing. (a) Schematic detailing the fabrication and integration of resonators and textile LIG sensors. (b) Mounting of LIG strain sensors on the shoulder, elbow, and wrist connected to an NFC hub and communicating wirelessly through textile-integrated waveguides. (c) Human subject motion resulting in (d) sensor data showing sequential bending of the wrist, elbow, and shoulder, followed by simultaneous bending of all three joints.

board is constructed using a commercially available NFC transponder chip, which includes an analog-to-digital converter (ADC) unit that connects to the strain sensors (Figure S9). To minimize the resistive strain and temperature sensor's hysteresis and random noise, we implemented a data processing algorithm for each sensor value in real-time and a few seconds after the start of each recording (Figure S10). This approach effectively achieved steady data with minimal noise fluctuations. The final clothing exhibits built-in, multipositional measurement capabilities while remaining completely flexible and lightweight owing to no batteries.

We utilized our LIG-enabled "smart" clothing for arm posture detection with strain sensors placed on the arm's shoulder, elbow joint, and wrist sections (Figure 5c,d). The strain sensor exhibits a sufficiently rapid response (up to 7 Hz, 30% strain; Figure S11) to capture general body motions. Strain sensors were calibrated by measuring the relative resistance change under varying bending angles (Figure S12), allowing us to correlate the sensor response with arm angles and posture. Upon applying the sensor and BAN networks to the human arm, multinode posture monitoring was conducted (Figure 5c,d) with a single NFC reader affixed using an armband. After an initial data acquisition/calibration phase i,

repeated posture monitoring was performed in stages ii, iii, iv, and v, involving distinct movements of the wrist, elbow, and shoulder joints with specific angles. The network's efficiency was evaluated by recording the packet reception ratio (PRR) during the activity, which was found to be reliable with a value above 95% (Figure 5d). This not only underscores the robustness of the network but also accentuates the seamless signal communication facilitated by the surface propagation characteristics inherent to this magneto-inductive structure.

These results demonstrate that the clothing could effectively differentiate between distinct motions, adding layers of intelligence to wearable tech. Our LIG-enabled "smart" clothing stands out as a cost-effective, adaptable alternative, paving the way for tailoring wearable networks to individual needs.

# CONCLUSIONS

In conclusion, we have successfully developed LIG-based, integrated, multiparameter "smart" textiles for wireless, cross-body metrics. Versatile, selective sensors are incorporated into textiles by using cost-effective integration steps with tunable multilayers and simple heat-pressing. Such adaptable sensors offer user-friendly, low-burden solutions for a wide range of

applications in body tracking and body metric monitoring. Sensors are readily cobuilt with textile-integrated magnetic metamaterials, ultimately forming battery-free sensor networks that are adaptable across applications and people. The modular nature of this platform is expected to foster broader practical prospects for in situ health monitoring as a low-cost, customizable solution for personalized wearable networks. The potential applications of this system are manifold, encompassing posture analysis, human tracking mechanisms, assessments of athletic performances and everyday activities, real-time health, and status surveillance.

#### EXPERIMENTAL SECTION

**Materials.** Polyimide (PI) Kapton tape was obtained from DuPont, Inc. Heat press paper was acquired from the AVERY Store, while the Ecoflex fast cure silicone rubber compound kit was purchased from the Smooth-On Store.

**LIG Conversion or LIG Formation.** A laser cutter (VLS2.30, Versa laser) equipped with a  $10.6~\mu m$  pulsed CO<sub>2</sub> laser was used to pattern the PI film. The PI film with a thickness of  $100~\mu m$  was cleaned with ethanol before carving to induce graphene formation. The sensor design was produced by using AutoCAD (Autodesk 2022, USA). The subsequent raster-scan-based lasing operation was carried out at a pulse separation of  $25.4~\mu m$  (1000~ppi). The laser power was carefully adjusted to suit different sensor requirements, and a scan speed of  $10~mm~s^{-1}$  was maintained throughout the process. Various patterned textile sensors were produced by controlling the laser's motion along the X-Y axis. The subsequent sections detail the specific preparation processes for each type of LIG sensor.

**Preparation of LIG-Strain Sensor.** A  $2.5 \times 1~\rm cm^2$  area of PI film was patterned at a constant speed of 10 mm s<sup>-1</sup> and using a laser power of 2.375 W. After forming various patterns, the LIG-strain sensor was connected using a copper sheet and silver paste. The sensor was then encapsulated with silicone (Ecoflex) and heat-pressed onto the textile for 30 s at 220 °C. To eliminate noise from strain and other motions, a 3D-printed polylactic acid (PLA) platform was securely attached to the textile's backside.

**Preparation of LIG-Humidity Sensor.** The humidity sensor was patterned into a  $1 \times 1$  cm<sup>2</sup> square shape. After pattern formation, the LIG-humidity sensor was connected by using a copper sheet and silver paste. Liquid electrical tape was applied to the silver paste to protect the electronic connection from humidity. The sensor was heat pressed onto the textile for 30 s at 220 °C. To eliminate noise from strain and other motions, a 3D-printed PLA platform was securely attached to the textile's backside.

**Preparation of LIG-Temperature Sensor.** The temperature sensor was patterned into a  $1 \times 1$  cm<sup>2</sup> square shape. After the pattern was formed, the LIG-temperature sensor was connected using copper wire and silver paste. The sensor was encapsulated with Ecoflex and heat pressed onto the textile for 30 s at 220 °C. To isolate the sensor from strain and other motion-induced noise, a 3D-printed PLA platform was firmly attached to the textile's backside.

Resonator Fabrication. Grounded resonators were fabricated by stacking a copper sheet (25  $\mu$ m thick) on a transparent self-adhesive vinyl-film substrate. Similarly, we used aluminum foil (14  $\mu$ m thick) for the ground layer. The metal/vinyl layers were stacked on the adhesive cutting mat and cut using a Silhouette Cameo 3 system (Silhouette America). The complementary pattern of the metal foil was etched after cutting. Then, the top aluminum surface of the ground stack was coated with a general-purpose adhesive spray. The coil (copper/vinyl stack) was then aligned and placed on top of the adhesive-coated surface of the ground layer (aluminum/vinyl stack) after 1 min. The final stack (copper/vinyl/aluminum/vinyl) was then immediately covered by inflammable fabric and heat pressed under 260 °F for 45 s and allowed to cool afterward. The adhesive coating should be uniform and controlled to avoid resonance frequency shifts. The resonance behavior of the coils was then measured and tuned with a vector network analyzer (E5063A, Keysight) through a loop

reader antenna to ensure that all elements resonate at 13.56 MHz to achieve the maximum transmission. As Optionally, an additional transparent vinyl layer may be placed on top of the resonator (adhesive-facing copper) to seal the resonator and enhance the mechanical and waterproof properties.

**Textile Sensor Integration.** After positioning the resonators on the clothing, a heat-transfer vinyl (transparent or opaque, depending on design preference) was cut and placed on top. The assembly was then heat pressed at 300 °F for 1 min and allowed to cool. Once the resonators and textile sensors were securely affixed to the cloth, a near-field communications (NFC) component was integrated with the sensor using a mini-micro-pin connector plug. The serpentine-shaped copper sheet connector was threaded through a precut hole in the transfer vinyl and plugged into a micro-pin connector. The other end of this connector was already connected to the NFC component.

Raman Spectroscopy. Raman spectroscopy measurements were conducted using a Guildenstern dark field/remand/fluorescence microscopy system (Guildenstern Technologies, Inc.). Samples were prepared by depositing a thin layer of the LIG sample onto a clean glass slide. The slide was then mounted onto the microscope stage, and the system was adjusted to achieve optimal focus and alignment. Darkfield microscopy was utilized to identify and locate the areas of interest in the sample. For Raman spectroscopy, the system was equipped with a 532 nm excitation laser, which was directed at the sample through a high numerical aperture (NA) objective lens. The Raman scattered light from the sample was collected by the same objective lens and then spectrally dispersed using a high-resolution spectrometer. The resulting Raman spectrum was acquired using a thermoelectrically cooled charge-coupled device (CCD) detector. Spectra were recorded over the range of 100-3200 cm<sup>-1</sup> with a spectral resolution of approximately 1 cm<sup>-1</sup>. For each measurement, an acquisition time of 10 s and an accumulation of 3 scans were used to obtain a high-quality Raman spectrum.

**Resistance Measurements.** A rectangular pattern measuring  $1 \times 0.3$  cm was designed using AutoCAD and imported into the laser scribing system. The pattern was then printed onto PI film attached to heat transfer tape. Following the printing procedure, a digital multimeter was employed to measure the electrical resistance of each printed pattern. By ensuring secure contact between the multimeter probes and the pattern edges, accurate resistance values were obtained.

Scanning Electron Microscopy. Scanning electron microscopy (SEM) was performed using a Hitachi 4700 field emission scanning electron microscope (Hitachi High-Technologies Corporation). The LIG sample was mounted onto a SEM-compatible stub by using conductive adhesive tape. The samples were then sputter-coated with a thin layer of Ir to enhance the conductivity and minimize charging effects during imaging. Once coated, the samples were transferred to the microscope's vacuum chamber and secured to the stage. During imaging, the microscope was operated in high-vacuum mode to maintain optimal imaging conditions and prevent contamination of the electron column. Image acquisition and processing were carried out using integrated software, enabling real-time adjustments of focus, magnification, and contrast.

**Strain Experiments.** Strain characterization measurements were performed using a Zaber linear motion control system. A precision LCR meter (Keysight E4980AL) was concurrently employed to measure the resistance change of the sensor as a function of strain. The initial distance between the clamps of the tensile testing machine was set to 2.5 cm. The cycle test was performed under a strain of 2.5% for 1000 cycles.

Humidity Experiments. A precision LCR meter (Keysight E4980AL) was employed to measure the resistance change of the sensor as a function of humidity. An ultrasonic humidification system (Electro-Tech Systems, Inc.) was used to facilitate the calibration of the humidity experiments. The humidity sensor was positioned vertically against the wall of the humidity chamber, ensuring accurate and consistent exposure to the controlled humidity environment. Simultaneously, a separate humidity sensor monitored the chamber's humidity levels. For static experiments, the ultrasonic humidifier

within the chamber generated water vapor, subsequently altering the humidity levels surrounding the sensor. By systematically varying the humidity levels and monitoring the sensor's resistance change, the sensor's sensitivity and response to different humidity conditions were thoroughly assessed. On-body experiments were performed to evaluate the sensor's performance during real-world use. Test subjects wore clothing embedded with the humidity sensor, and the sensor's response to changes in humidity was characterized in situ.

Temperature Experiments. A heat plate was utilized to provide a controlled-temperature environment for sensor calibration. A rectangular Ecoflex buffer was used between the sensor and the hot plate to protect the sensor. A precision LCR meter (Keysight E4980AL) was employed to measure the resistance change of the sensor's resistance as a function of temperature. An infrared (IR) thermometer (Fluke Corporation) was used to measure the surface temperature of the Ecoflex stage. The temperature sensor was attached to the surface of the Ecoflex stage, and the resistance was measured while the temperature was gradually increased using the heat plate. For static experiments, a preheated Ecoflex stage was gently touched to the temperature sensor and subsequently released. On-body experiments were performed to evaluate the sensor's performance during real-world use. Test subjects wore clothing embedded with the temperature sensor, and the sensor's response to changes in body temperature was characterized in situ.

Motion Experiments. Motion experiments were conducted to evaluate the performance and sensitivity of the sensor in response to body movements. A precision LCR meter (Keysight E4980AL) was employed to measure the resistance change of the sensor during various motion activities. Wrist braces (NEO-G) and elbow sleeves were used to serve as test garments for these experiments. The LIG strain sensor, affixed with heat transfer tape, was heat pressed onto designated areas of the wrist brace (on the back of the wrist) and the elbow sleeve (on the medial and lateral aspects of the elbow). Throughout the motion experiments, test subjects wore the wrist brace and elbow sleeve while performing a range of movements, including flexion, extension, and rotation. The resistance changes of the LIG strain sensor, induced by these motions, were continuously monitored by using the LCR meter.

#### ASSOCIATED CONTENT

## Supporting Information

The Supporting Information is available free of charge at https://pubs.acs.org/doi/10.1021/acsanm.3c03582.

LIG sensor assembly and cross-section; visual representation of PI-to-LIG conversion; surface morphology of LIG porous structure; sensitivity characterization; pulse measurements from LIG strain sensor; reusability characterization; sensor reproducibility; simultaneous temperature and humidity sensing during motion LIG strain sensor calibration for BAN integration; NFC transponder flexible circuit board design; flowchart for software-based TDMA and sensor data processing; LIG strain sensor response rate; and LIG strain sensor calibration for BAN (PDF)

## AUTHOR INFORMATION

## **Corresponding Author**

Peter Tseng — Material and Manufacturing Technology Program, Department of Biomedical Engineering, and Center for Embedded and Cyber-physical Systems, University of California, Irvine, California 92617, United States; Email: tsengpc@uci.edu

#### **Authors**

Huiting Qin – Department of Electrical Engineering and Computer Science, University of California, Irvine, California 92617, United States; Material and Manufacturing Technology Program, University of California, Irvine, California 92617, United States

Amirhossein Hajiaghajani – Material and Manufacturing Technology Program, University of California, Irvine, California 92617, United States

Alberto Ranier Escobar — Department of Biomedical Engineering, University of California, Irvine, California 92617, United States; orcid.org/0000-0002-0381-1699

Amir Hosein Afandizadeh Zargari – Material and Manufacturing Technology Program and Center for Embedded and Cyber-physical Systems, University of California, Irvine, California 92617, United States

Abel Jimenez – Material and Manufacturing Technology Program, University of California, Irvine, California 92617, United States

Fadi Kurdahi – Department of Electrical Engineering and Computer Science, University of California, Irvine, California 92617, United States; Center for Embedded and Cyberphysical Systems, University of California, Irvine, California 92617, United States

Complete contact information is available at: https://pubs.acs.org/10.1021/acsanm.3c03582

#### **Notes**

The authors declare no competing financial interest.

#### ACKNOWLEDGMENTS

The authors acknowledge funding from the National Science Foundation (NSF) Career Award (award no. 1942364) for supporting this work. We acknowledge Laser Spectroscopy Laboratories at the University of California, Irvine. The authors also acknowledge the use of facilities and instrumentation at the UC Irvine Materials Research Institute (IMRI), which is supported in part by the National Science Foundation through the UC Irvine Materials Research Science and Engineering Center (DMR-2011967). The authors also thank C.Q. and X.C. from The Khine Lab for training in instrumentation.

### REFERENCES

- (1) Jeong, I. C.; Bychkov, D.; Searson, P. C. Wearable Devices for Precision Medicine and Health State Monitoring. *IEEE Trans. Biomed. Eng.* **2019**, *66* (5), 1242–1258.
- (2) Tipparaju, V. V.; Wang, D.; Yu, J. J.; Chen, F.; Tsow, F.; Forzani, E.; Tao, N.; Xian, X. Respiration pattern recognition by wearable mask device. *Biosens. Bioelectron.* **2020**, *169*, 112590.
- (3) Pumera, M. Graphene in biosensing. *Mater. Today* **2011**, *14* (7–8), 308–315.
- (4) Doria, G.; Conde, J.; Veigas, B.; Giestas, L.; Almeida, C.; Assuncao, M.; Rosa, J.; Baptista, P. V. Noble Metal Nanoparticles for Biosensing Applications. *Sensors* **2012**, *12* (2), 1657–1687.
- (5) Ray, T. R.; Choi, J.; Bandodkar, A. J.; Krishnan, S.; Gutruf, P.; Tian, L. M.; Ghaffari, R.; Rogers, J. A. Bio-Integrated Wearable Systems: A Comprehensive Review. *Chem. Rev.* **2019**, *119* (8), 5461–5533.
- (6) Wang, X. W.; Liu, Z.; Zhang, T. Flexible Sensing Electronics for Wearable/Attachable Health Monitoring. *Small* **2017**, *13* (25), 1602790.
- (7) Gao, W.; Emaminejad, S.; Nyein, H. Y. Y.; Challa, S.; Chen, K. V.; Peck, A.; Fahad, H. M.; Ota, H.; Shiraki, H.; Kiriya, D.; Lien, D. H.; Brooks, G. A.; Davis, R. W.; Javey, A. Fully integrated wearable sensor arrays for multiplexed in situ perspiration analysis. *Nature* **2016**, *529* (7587), 509–514.

- (8) Fu, C. Y.; Tang, W. Y.; Miao, Y.; Xu, A.; Nilghaz, A.; Xu, W.; Dong, K.; Su, B.; Xia, Z. Large-scalable fabrication of liquid metal-based double helix core-spun yarns for capacitive sensing, energy harvesting, and thermal management. *Nano Energy* **2023**, *106*, 108078.
- (9) Tang, J.; Wu, Y. T.; Ma, S. D.; Yan, T.; Pan, Z. J. Flexible strain sensor based on CNT/TPU composite nanofiber yarn for smart sports bandage. *Composites, Part B* **2022**, 232, 109605.
- (10) Wei, Y. H.; Li, X. S.; Wang, Y. F.; Hirtz, T.; Guo, Z. F.; Qiao, Y. C.; Cui, T. R.; Tian, H.; Yang, Y.; Ren, T. L. Graphene-Based Multifunctional Textile for Sensing and Actuating. *ACS Nano* **2021**, 15 (11), 17738–17747.
- (11) Liu, W.; Huang, Y. H.; Peng, Y. D.; Walczak, M.; Wang, D.; Chen, Q.; Liu, Z.; Li, L. Stable Wearable Strain Sensors on Textiles by Direct Laser Writing of Graphene. *ACS Appl. Nano Mater.* **2020**, 3 (1), 283–293.
- (12) Wang, L.; Fu, X. M.; He, J. Q.; Shi, X.; Chen, T. Q.; Chen, P.; Wang, B.; Peng, H. Application Challenges in Fiber and Textile Electronics. *Adv. Mater.* **2020**, 32 (5), 1901971.
- (13) Lee, J.; Llerena Zambrano, B.; Woo, J.; Yoon, K.; Lee, T. Recent Advances in 1D Stretchable Electrodes and Devices for Textile and Wearable Electronics: Materials, Fabrications, and Applications. *Adv. Mater.* **2020**, 32 (5), 1902532.
- (14) Dhanabalan, S. C.; Dhanabalan, B.; Chen, X.; Ponraj, J. S.; Zhang, H. Hybrid carbon nanostructured fibers: stepping stone for intelligent textile-based electronics. *Nanoscale* **2019**, *11* (7), 3046–3101.
- (15) Yang, Z.; Pang, Y.; Han, X. L.; Yang, Y. F.; Ling, J.; Jian, M. Q.; Zhang, Y. Y.; Yang, Y.; Ren, T. L. Graphene Textile Strain Sensor with Negative Resistance Variation for Human Motion Detection. *ACS Nano* **2018**, *12* (9), 9134–9141.
- (16) Liu, L. B.; Yu, Y.; Yan, C.; Li, K.; Zheng, Z. J. Wearable energy-dense and power-dense supercapacitor yarns enabled by scalable graphene-metallic textile composite electrodes. *Nat. Commun.* **2015**, *6*, 7260.
- (17) Hajiaghajani, A.; Tseng, P. Microelectronics-Free, Augmented Telemetry from Body-Worn Passive Wireless Sensors. *Adv. Mater. Technol.* **2021**, *6* (4), 2001127.
- (18) Jao, Y. T.; Yang, P. K.; Chiu, C. M.; Lin, Y. J.; Chen, S. W.; Choi, D.; Lin, Z. H. A textile-based triboelectric nanogenerator with humidity-resistant output characteristic and its applications in self-powered healthcare sensors. *Nano Energy* **2018**, *50*, 513–520.
- (19) He, T. Y. Y.; Shi, Q. F.; Wang, H.; Wen, F.; Chen, T.; Ouyang, J. Y.; Lee, C. Beyond energy harvesting multi-functional triboelectric nanosensors on a textile. *Nano Energy* **2019**, *57*, 338–352.
- (20) Zhang, L.; He, J.; Liao, Y. S.; Zeng, X. T.; Qiu, N. X.; Liang, Y.; Xiao, P.; Chen, T. A self-protective, reproducible textile sensor with high performance towards human-machine interactions. *J. Mater. Chem. A* **2019**, 7 (46), 26631–26640.
- (21) Tian, X.; Lee, P. M.; Tan, Y. J.; Wu, T. L. Y.; Yao, H. C.; Zhang, M. Y.; Li, Z. P.; Ng, K. A.; Tee, B. C. K.; Ho, J. S. Wireless body sensor networks based on metamaterial textiles. *Nat. Electron.* **2019**, 2 (6), 243–251.
- (22) Angelucci, A.; Cavicchioli, M.; Cintorrino, I.; Lauricella, G.; Rossi, C.; Strati, S.; Aliverti, A. Smart Textiles and Sensorized Garments for Physiological Monitoring: A Review of Available Solutions and Techniques. *Sensors* **2021**, *21* (3), 814.
- (23) Zaman, S. u.; Tao, X.; Cochrane, C.; Koncar, V. Smart E-Textile Systems: A Review for Healthcare Applications. *Electronics* **2021**, *11* (1), 99.
- (24) Dias, D.; Paulo Silva Cunha, J. Wearable Health Devices-Vital Sign Monitoring, Systems and Technologies. *Sensors* **2018**, *18* (8), 2414.
- (25) Nowell, L. S.; Norris, J. M.; White, D. E. Thematic Analysis: Striving to Meet the Trustworthiness Criteria. *Int. J. Qual. Methods* **2017**, *16* (1), 1609406917733847.
- (26) Du, K.; Lin, R.; Yin, L.; Ho, J. S.; Wang, J.; Lim, C. T. Electronic textiles for energy, sensing, and communication. *iScience* **2022**, 25 (5), 104174.

- (27) Zheng, Y. J.; Li, Y. L.; Zhou, Y. J.; Dai, K.; Zheng, G. Q.; Zhang, B.; Liu, C. T.; Shen, C. Y. High-Performance Wearable Strain Sensor Based on Graphene/Cotton Fabric with High Durability and Low Detection Limit. ACS Appl. Mater. Interfaces 2020, 12 (1), 1474–1485
- (28) Dulal, M.; Afroj, S.; Ahn, J.; Cho, Y.; Carr, C.; Kim, I. D.; Karim, N. Toward Sustainable Wearable Electronic Textiles. *ACS Nano* **2022**, *16* (12), 19755–19788.
- (29) Lin, J.; Peng, Z.; Liu, Y.; Ruiz-Zepeda, F.; Ye, R.; Samuel, E. L. G.; Yacaman, M. J.; Yakobson, B. I.; Tour, J. M. Laser-induced porous graphene films from commercial polymers. *Nat. Commun.* **2014**, *5*, 5714.
- (30) Le, T. D.; Phan, H.; Kwon, S.; Park, S.; Jung, Y.; Min, J.; Chun, B. J.; Yoon, H.; Ko, S. H.; Kim, S.; et al. Recent Advances in Laser-Induced Graphene: Mechanism, Fabrication, Properties, and Applications in Flexible Electronics. *Adv. Funct. Mater.* **2022**, 32 (48), 2205158.
- (31) He, M. H.; Wang, G. T.; Zhu, Y. X.; Wang, Y. A.; Liu, F.; Luo, S. D. In-situ joule heating-triggered nanopores generation in laser-induced graphene papers for capacitive enhancement. *Carbon* **2022**, *186*, 215–226.
- (32) Zhang, J.; Ren, M.; Wang, L.; Li, Y.; Yakobson, B. I.; Tour, J. M. Oxidized Laser-Induced Graphene for Efficient Oxygen Electrocatalysis. *Adv. Mater.* **2018**, *30* (21), 1707319.
- (33) Ren, M. Q.; Zhang, J. B.; Tour, J. M. Laser-induced graphene synthesis of Co3O4 in graphene for oxygen electrocatalysis and metalair batteries. *Carbon* **2018**, *139*, 880–887.
- (34) Liu, W.; Chen, Q.; Huang, Y. H.; Wang, D.; Li, L.; Liu, Z. In situ laser synthesis of Pt nanoparticles embedded in graphene films for wearable strain sensors with ultra-high sensitivity and stability. *Carbon* **2022**, *190*, 245–254.
- (35) Chen, X.; Hou, Z.; Li, G.; Yu, W.; Xue, Y.; Niu, G.; Xin, M.; Yang, L.; Meng, C.; Guo, S. A laser-scribed wearable strain sensing system powered by an integrated rechargeable thin-film zinc-air battery for a long-time continuous healthcare monitoring. *Nano Energy* **2022**, *101*, 107606.
- (36) Xu, K.; Fujita, Y.; Lu, Y.; Honda, S.; Shiomi, M.; Arie, T.; Akita, S.; Takei, K. A Wearable Body Condition Sensor System with Wireless Feedback Alarm Functions. *Adv. Mater.* **2021**, 33 (18), 2008701.
- (37) Gupta, A.; Sharma, C. P.; Thamaraiselvan, C.; Pisharody, L.; Powell, C. D.; Arnusch, C. J. Low-Voltage Bacterial and Viral Killing Using Laser-Induced Graphene-Coated Non-woven Air Filters. *ACS Appl. Mater. Interfaces* **2021**, *13* (49), 59373–59380.
- (38) Chyan, Y.; Ye, R. Q.; Li, Y. L.; Singh, S. P.; Arnusch, C. J.; Tour, J. M. Laser-Induced Graphene by Multiple Lasing: Toward Electronics on Cloth, Paper, and Food. *ACS Nano* **2018**, *12* (3), 2176–2183.
- (39) Luong, D. X.; Yang, K. C.; Yoon, J.; Singh, S. P.; Wang, T.; Arnusch, C. J.; Tour, J. M. Laser-Induced Graphene Composites as Multifunctional Surfaces. *ACS Nano* **2019**, *13* (2), 2579–2586.
- (40) Lin, S. Y.; Feng, W. D.; Miao, X. F.; Zhang, X. X.; Chen, S. J.; Chen, Y. Q.; Wang, W.; Zhang, Y. N. A flexible and highly sensitive nonenzymatic glucose sensor based on DVD-laser scribed graphene substrate. *Biosens. Bioelectron.* **2018**, *110*, 89–96.
- (41) Rajaji, U.; Ganesh, P. S.; Kim, S. Y.; Govindasamy, M.; Alshgari, R. A.; Liu, T. Y. MoS2 Sphere/2D S-Ti3C2MXene Nanocatalysts on Laser-Induced Graphene Electrodes for Hazardous Aristolochic Acid and Roxarsone Electrochemical Detection. *ACS Appl. Nano Mater.* **2022**, *5* (3), 3252–3264.
- (42) Liu, X.; Cheng, H.; Zhao, Y.; Wang, Y.; Li, F. Portable electrochemical biosensor based on laser-induced graphene and MnO2 switch-bridged DNA signal amplification for sensitive detection of pesticide. *Biosens. Bioelectron.* 2022, 199, 113906.
- (43) Rajaji, U.; Govindasamy, M.; Sha, R.; Alshgari, R. A.; Juang, R. S.; Liu, T. Y. Surface engineering of 3D spinel Zn3V2O8 wrapped on sulfur doped graphitic nitride composites: Investigation on the dual role of electrocatalyst for simultaneous detection of antibiotic drugs in biological fluids. *Composites, Part B* **2022**, 242, 110017.

(44) Wang, H. M.; Wang, H. M.; Wang, Y. L.; Su, X. Y.; Wang, C. Y.; Zhang, M. C.; Jian, M. Q.; Xia, K. L.; Liang, X. P.; Lu, H. J.; Li, S.; Zhang, Y. Y. Laser Writing of Janus Graphene/Kevlar Textile for Intelligent Protective Clothing. ACS Nano 2020, 14 (3), 3219-3226. (45) Raza, T.; Tufail, M. K.; Ali, A.; Boakye, A.; Qi, X.; Ma, Y.; Ali,

A.; Qu, L.; Tian, M. Wearable and Flexible Multifunctional Sensor Based on Laser-Induced Graphene for the Sports Monitoring System. ACS Appl. Mater. Interfaces 2022, 14 (48), 54170-54181.

- (46) Yang, L.; Ji, H. D.; Meng, C. Z.; Li, Y. H.; Zheng, G. H.; Chen, X.; Niu, G. Y.; Yan, J. Y.; Xue, Y.; Guo, S. J.; Cheng, H. Y. Intrinsically Breathable and Flexible NO2 Gas Sensors Produced by Laser Direct Writing of Self-Assembled Block Copolymers. ACS Appl. Mater. Interfaces 2022, 14 (15), 17818-17825.
- (47) Parmeggiani, M.; Stassi, S.; Fontana, M.; Bianco, S.; Catania, F.; Scaltrito, L.; Lamberti, A. Laser-induced graphenization of textile yarn for wearable electronics application. Smart Mater. Struct. 2021, 30 (10), 105007.
- (48) Hajiaghajani, A.; Afandizadeh Zargari, A. H.; Dautta, M.; Jimenez, A.; Kurdahi, F.; Tseng, P. Textile-integrated metamaterials for near-field multibody area networks. Nat. Electron. 2021, 4 (11), 808-817.
- (49) Wang, H.; Zhao, Z.; Liu, P.; Guo, X. A soft and stretchable electronics using laser-induced graphene on polyimide/PDMS composite substrate. npj Flexible Electron. 2022, 6 (1), 26.
- (50) Chen, X.; Luo, F.; Yuan, M.; Xie, D.; Shen, L.; Zheng, K.; Wang, Z.; Li, X.; Tao, L. A Dual-Functional Graphene-Based Self-Alarm Health-Monitoring E-Skin. Adv. Funct. Mater. 2019, 29 (51),
- (51) Ji, B. W.; Xie, Z. Q.; Hong, W.; Jiang, C. P.; Guo, Z. J.; Wang, L. C.; Wang, X. L.; Yang, B.; Liu, J. Q. Stretchable Parylene-C electrodes enabled by serpentine structures on arbitrary elastomers by silicone rubber adhesive. J. Materiomics 2020, 6 (2), 330-338.